# A Novel Vibration Control Strategy for Active Magnetic Bearing-based Motor Drive with Displacement Harmonic Injection

Fan Longyuan*, Liu Zicheng **, Wang Haijiao**, Zhang Jiong**, and Jiang Dong**
*Institute of Artificial Intelligence, Huazhong University of Science and Technology
4-1 Wuhan, China
E-mail: flyin@hust.edu.cn
** School of Electrical and Electronic Engineering, Huazhong University of Science and Technology
4-1 Wuhan, China

**Abstract**
This paper proposes a novel vibration suppression strategy based on displacement harmonic injection to mitigate prominent rotational frequency vibrations in AMB-based motor drives, with the goal of improving rotor eccentricity and reducing electromagnetic vibrations. First, the impact of rotor eccentricity on the motor system's electromagnetic vibrations is analyzed, revealing the mechanism behind rotational frequency vibrations. Next, the influence of manufacturing errors on displacement control accuracy is discussed, and an error compensation strategy is introduced to enhance the system's response to imbalance and improve rotor performance through dynamically adjusted reference commands. Experimental results demonstrate the effectiveness of the proposed method, with the motor's rotational frequency vibration acceleration reduced by 98.1% compared to traditional PID control and by 87.5% compared to conventional displacement vibration suppression techniques.

***Keywords*** : Active magnetic bearing (AMB), Vibration control, Rotor eccentricity, Machining errors, Displacement harmonic injection

## 1. Introduction

Active magnetic bearings (AMBs) offer key advantages, including contactless operation, no lubrication, low energy loss, high precision, and real-time active control. These features have enabled their widespread use in various industrial applications (Prasad & Narayanan, 2021; Ma et al., 2023). In particular, AMB-based motor systems hold significant promise for low-speed, heavy-load applications in marine propulsion systems (Ahad & Ahmad, 2021; Lewis et al., 1989). Reducing electromagnetic vibration and noise is crucial during ship operation. However, the electromagnetic vibration spectra at the rotational frequencies of AMB-driven motor systems are pronounced and challenging to mitigate using passive vibration isolation methods. As the source of vibration and noise, the AMB motor system's precise control of electromechanical characteristics offers potential for active vibration suppression.

Current research on AMB active vibration control primarily focuses on two methods: current vibration suppression and displacement vibration suppression. Current vibration suppression (also known as automatic balance control) reduces harmonic components in the control current at the rotational frequency by filtering out rotor imbalance from the displacement feedback signal. Common techniques include generalized notch filtering (Peng et al., 2018), least mean squares (Liu et al., 2020), resonance control (Ren et al., 2023), and repetitive control (Cui et al., 2016). Displacement vibration suppression (i.e., imbalance compensation) eliminates rotor displacement vibrations by adjusting control currents or imbalance forces, ensuring the rotor rotates around its geometric center. Typical methods include iterative learning control (Chuan & Changsheng, 2018), repetitive control (Han et al., 2015), sliding mode control (Chen et al., 2020), and second-order generalized integrators (Sun et al., 2021).

Existing AMB vibration control strategies face two main limitations: First, traditional vibration control strategies for magnetic bearings focus solely on rotor displacement vibration and control current, neglecting the impact of rotor displacement changes on the stator air-gap electromagnetic forces, thus failing to effectively assess motor vibration.

Second, many AMB vibration control systems fail to account for rotor manufacturing errors, reducing control accuracy and degrading rotor performance. While some studies have examined machining error identification and its influence on rotor behavior (Kim & Lee, 1997; Rossner et al., 2015), effective control remains challenging due to the coupling of these errors with rotor imbalance (Zhang et al., 2021). Additionally, the lack of a clear evaluation index makes it difficult to quantify the effectiveness of error compensation.

This paper addresses these challenges by analyzing the excitation mechanism of rotor displacement fluctuations (e.g., eccentricity) and their effect on air-gap magnetic reluctance and electromagnetic force waves. The study identifies the primary frequency components and spatial orders of electromagnetic vibration caused by rotor eccentricity, providing a foundation for designing vibration reduction algorithms. Furthermore, we propose a novel AMB vibration control strategy that incorporates material defects and manufacturing errors to achieve precise rotor position control, thereby mitigating eccentricity and significantly improving the vibration performance of AMB motor systems.

## 2. Electromagnetic force analysis under rotor eccentricity

A typical five-degree-of-freedom (5-DOF) AMB system is shown in Fig. 1. It consists of two radial magnetic bearings, one axial magnetic bearing, and a permanent magnet synchronous motor (PMSM).

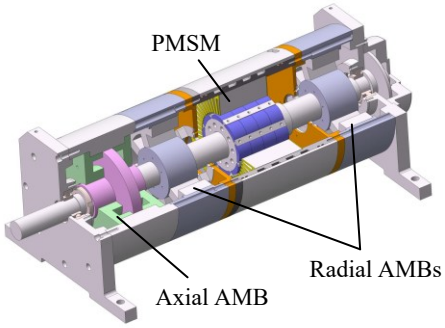


Fig. 1 5-DOF AMB assembly

In the no-load condition of the PMSM, the air-gap magnetomotive force (MMF) is generated by the permanent magnets, and can be expressed as:

$$F_{PM}(\theta,t)=\sum_{u}^{\infty}F_u\cos up(\theta-\omega_m t) \tag{1}$$

where $p$ is the number of pole pairs, $u$ represents the harmonic order of the permanent magnet MMF, $u$=2$k$-1, $k$=1,2,3..., and $\omega_m$ is the mechanical angular velocity of the motor.

Rotor eccentricity refers to the misalignment of the rotor due to mechanical processing and assembly errors. The two common types of rotor eccentricity are static and dynamic, as shown in Fig. 2, where $O$ and $O'$ represent the geometric centers of the stator and rotor, respectively. During static eccentricity, the air-gap length changes with the circumferential position. In dynamic eccentricity, the rotor's center of rotation deviates from its geometric center, causing periodic changes in the position of the minimum air-gap length during rotation. When rotor eccentricity occurs, the air-gap length can be expressed as:

$$g=g_0-e\cos(\theta-\omega_m t+\varphi_{ec}) \tag{2}$$

$$e=\sqrt{x^2(t)+y^2(t)} \tag{3}$$

$$\varphi_{ec}-\omega_m t=\arctan(\frac{y(t)}{x(t)}) \tag{4}$$

where $g_0$ is the air-gap length when there is no eccentricity, $e$ is the eccentricity distance, $\varphi$ is the initial phase of the eccentricity position, $\theta$ is the circumferential position, $\omega_m$ is the rotational angular velocity of the rotor axis relative to the stator axis after eccentricity. For static eccentricity, $\omega_m$=0; for dynamic eccentricity, $\omega_m$ is the mechanical angular velocity of the motor. $x$ and $y$ represent the displacement of the rotor center relative to the stator center. Ignoring core saturation and stator slots, the air-gap magnetic reluctance under rotor eccentricity can be expressed as:

$$\begin{aligned}\Lambda(\theta) &= \frac{\mu_0 A}{g_0 - e\cos(\theta - \omega_m t + \varphi_{ec})} \\ &\approx \Lambda_0 + \Lambda_0 \frac{e}{g_0}\cos(\theta - \omega_m t + \varphi_{ec})\end{aligned} \tag{5}$$

The first term of the equation, $\Lambda_0$, represents the air-gap magnetic reluctance when there is no rotor eccentricity. The second term indicates that eccentricity introduces a harmonic of air-gap magnetic reluctance with a spatial order of 1.

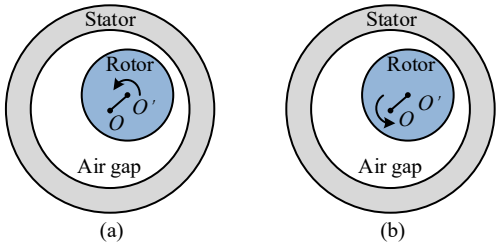


Fig. 2 Schematic diagrams of rotor eccentricity. (a) Static eccentricity. (b) Dynamic eccentricity

Thus, the radial magnetic flux density generated by the permanent magnet is expressed as:

$$\begin{aligned}B_r(\theta,t) &= F_{PM}(\theta,t)\cdot\Lambda(\theta) \\ &= \sum_u F_u \Lambda_0 \cos up(\theta - \omega_m t + \varphi_{ec}) \\ &+ \sum_u \frac{F_u \Lambda_0 e}{2g_0}\cos[(up\pm 1)\theta - (up\pm 1)\omega_m t + \varphi_{ec}]\end{aligned} \tag{6}$$

Due to the significantly larger radial component of the magnetic flux density in a permanent magnet motor compared to the tangential component, the tangential flux density is neglected in the calculation of electromagnetic force. Using the Maxwell stress tensor method, the radial electromagnetic force can be expressed as:

$$F_r = \frac{1}{2\mu_0}(B_r^2 - B_t^2) \approx \frac{1}{2\mu_0} B_r^2 \tag{7}$$

By combining equations (6) and (7), the harmonic expression for the air-gap electromagnetic force in a no-load permanent magnet motor is obtained. The amplitudes, spatial orders, and frequencies of the major components are listed in Table 1. It is evident that static eccentricity does not alter the temporal order of the radial electromagnetic force density but introduces new spatial orders. On the other hand, dynamic eccentricity introduces both new temporal and spatial orders.

The force waves with the largest amplitudes result from the interaction between the magnetic flux harmonics caused by eccentricity and the fundamental magnetic field ($u$=1), corresponding to Type 2 in the table, with spatial orders and temporal orders of ($v$=±1, $\omega$=±$\omega_m$) and ($v$=2$p$±1, $\omega$=2$p\omega_m$±$\omega_m$), respectively. This implies that eccentricity-induced electromagnetic force leads to significant vibrations at the 1st rotational frequency with a spatial order of 1.

Compared to conventional mechanical bearing motors, magnetic bearings offer enhanced spatial control over rotor displacement, providing the potential to improve rotor eccentricity conditions. Based on equations (2)-(4), it can be concluded that when the periodically varying components of radial rotor displacement $x$, $y$ are suppressed to zero, the rotor eccentricity shifts from dynamic to static, significantly reducing the electromagnetic vibration caused by dynamic eccentricity at the rotational frequency.

In the next section, we will introduce the control system of the AMB in detail.

Table 1
Electromagnetic Force Harmonics Introduced by Eccentricity

| Type | Amplitude | Spatial Order | Frequency |
|---|---|---|---|
| 1 | $\frac{F_{u1}F_{u2}\Lambda_0^{\,2}}{4\mu_0}$ | $(u_1\pm u_2)\,p$ | $(u_1\pm u_2)\,p\omega_m$ |
| 2 | $\frac{F_{u1}F_{u2}\Lambda_0^{\,2}e}{8g_0\mu_0}$ | $(u_1\pm u_2)\,p\pm1$ | $[(u_1\pm u_2)\,p\pm1]\omega_m$ |
| 3 | $\frac{F_{u1}F_{u2}\Lambda_0^{\,2}e^2}{16g_0\mu_0}$ | $(u_1\pm u_2)\,p\pm(1\pm1)$ | $[(u_1\pm u_2)\,p\pm(1\pm1)]\,\omega_m$ |

## 3. Control of the AMB system

### 3.1 Model of AMB

In the design of the AMB control system, differential control is commonly employed. This method generates opposing electromagnetic forces on each degree of freedom of the AMB through two symmetrically placed electromagnets. The rotor is stabilized and levitated by controlling the sum and difference of the bias current and the control current, respectively.

The resultant electromagnetic force formed by the upper and lower magnetic poles of each DOF is:

$$f_x = F_+ - F_- = \mu_0 A_a N^2 \cos\alpha\left(\frac{(i_0+i_x)^2}{(g_0+x)^2} - \frac{(i_0-i_x)^2}{(g_0-x)^2}\right) \approx k_i i_x - k_x x \tag{8}$$

After linearizing the resultant force at the bearing's equilibrium position, $k_i$ is the current stiffness coefficient, $k_x$ is the displacement stiffness coefficient (or negative stiffness of the bearing). $i_x$ denotes the control current, and $x$ represents the rotor's displacement along this DOF.

The rotor's dynamic motion equation and its Laplace transform are expressed as

$$m\ddot{x} = f_x + f_d \tag{9}$$

$$G(s) = \frac{x(s)}{i_x(s)} = \frac{k_i}{ms^2 + k_x} \tag{10}$$

where $m$ is the rotor mass, and $f_d$ is the disturbance force caused by mass imbalance. This disturbance induces a vibrational response at the rotational speed frequency, which can be expressed as $f_d = F_d \cos(\omega_m t+\theta)$.

Proportional-integral-differential (PID) control is widely used in AMB systems, and its transfer function is given by:

$$G_c(s) = k_P + \frac{k_I}{s} + k_D s \tag{11}$$

In conventional AMB control systems, PID control often fails to adequately respond to imbalance disturbances $f_d$, leading to significant rotor displacement fluctuations and increased rotor eccentricity, as discussed in Section II. Therefore, optimizing the vibration control strategy is necessary.

### 3.2 Proposed Vibration control Algrithm

To better align the constructed system model with the actual operating conditions of the magnetic bearing, the impact of sensor measurement errors should be taken into account. Due to material defects and rotor processing limitations, the

surface detected by the sensor becomes an irregular circle, resulting in measurement errors during displacement measurement, as shown in Fig. 3.

The measurement errors $x_e(t)$ can be expressed as (12)

$$x_e(t)=\begin{bmatrix}x_{elx}\\x_{erx}\\x_{ely}\\x_{ery}\end{bmatrix}=\begin{bmatrix}\sum_{i=1}^{n}\sigma_{li}\cos(i\omega_m t+\varphi_{li})\\\sum_{i=1}^{n}\sigma_{ri}\cos(i\omega_m t+\varphi_{ri})\\\sum_{i=1}^{n}\sigma_{li}\sin(i\omega_m t+\varphi_{li})\\\sum_{i=1}^{n}\sigma_{ri}\sin(i\omega_m t+\varphi_{ri})\end{bmatrix} \tag{12}$$

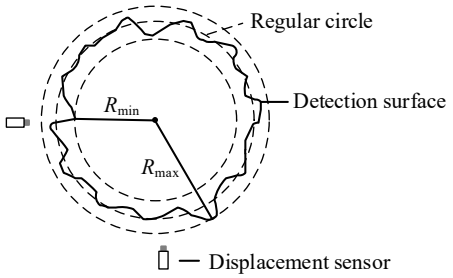


Fig. 3 Schematic diagram of detection roundness error.

where $i$ represents the harmonic order, $\sigma_{li}$ and $\sigma_{ri}$ are the displacement measurement error amplitudes for the left and right radial bearings, respectively, and $\varphi_{li}$ and $\varphi_{ri}$ are the corresponding initial phases.

Let $x_c(t)$ denote the actual displacement of the magnetic bearing. The displacement measured by the sensor can then be expressed as:

$$x(t)=x_c(t)+x_e(t) \tag{13}$$

To minimize the actual bearing displacement fluctuation $x_c$ , it is essential to consider both imbalance disturbances and sensor measurement errors in the control system. Accordingly, we have designed the AMB control block diagram, shown in Fig. 4. Firstly, we propose a feedforward compensation strategy based on phase-shift generalized integral (PSGI), which improves the system's response to imbalance disturbances. Its transfer function is given by (14). To address the error signal, we design the displacement reference signal $r(t)$ as a dynamic sine transformation, rather than zero, as shown in (15). When the frequency, amplitude, and phase of this signal match the actual processing errors $x_e$ described in (12), the actual bearing displacement $x_c$ is minimized.

$$G_{PSGI}(s)=\left(\varepsilon\cos\varphi+\frac{\varepsilon\Omega\sin\varphi}{s}\right)\frac{s}{s^2+\Omega^2} \tag{14}$$

$$r(t)=\sigma_e\cos(i\omega_m t+\phi) \tag{15}$$

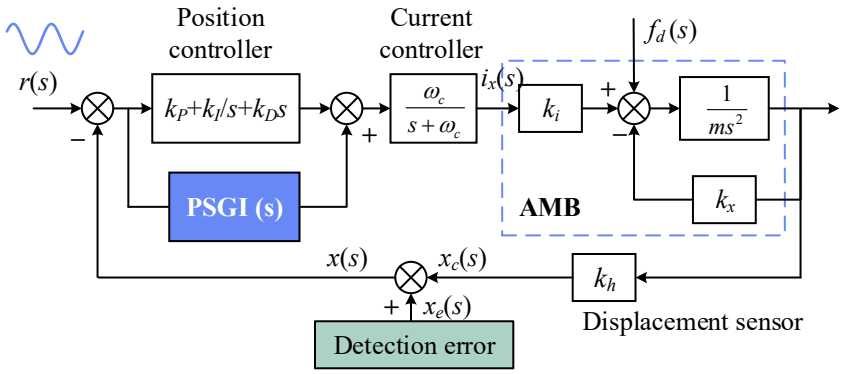


Fig. 4 Control block diagram of AMB.

## 4. Experimental Validation

To validate the effectiveness of the proposed vibration control strategy, we conducted experimental tests on a 5-DOF permanent magnet motor based on AMBs, as shown in Fig. 5. The vibration sensor used was the PCB352C68 model,

which detects vibration acceleration at the motor housing or foot. Vibration data were processed and analyzed using Siemens LMS Test.Lab software.

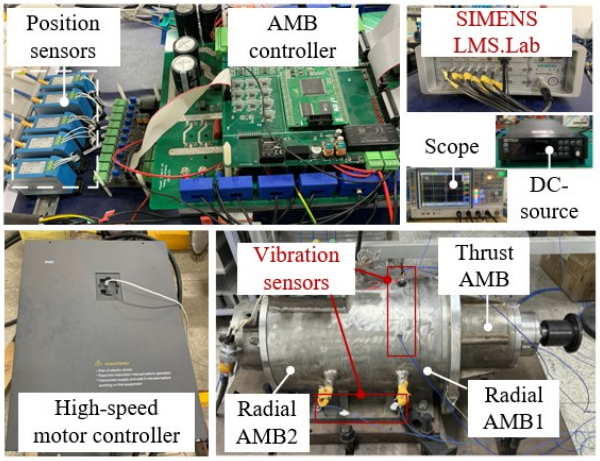


Fig. 5 Experimental setup.

Figure 6 illustrates the rotor displacement trajectories detected by radial AMB1 and AMB2 under conventional PID control, conventional vibration control (with the displacement reference signal set to 0), and the proposed displacement injection method. Under PID control, the rotor displacement fluctuates significantly between 40–60μm, primarily due to imbalance. While conventional vibration control (CVC) suppresses the detected displacement signal to zero, it fails to account for sensor runout. In contrast, the proposed approach injects rotary frequency signals with amplitudes of 13μm and 16μm into AMB1 and AMB2, respectively, compensating for machining-induced detection errors.

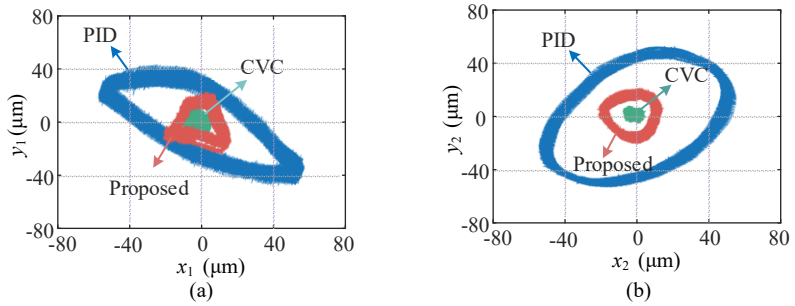


Fig. 6 Rotor displacement trajectories at 2400 rpm. (a) Displacement signals measured by AMB1. (b) Displacement signals measured by AMB2.

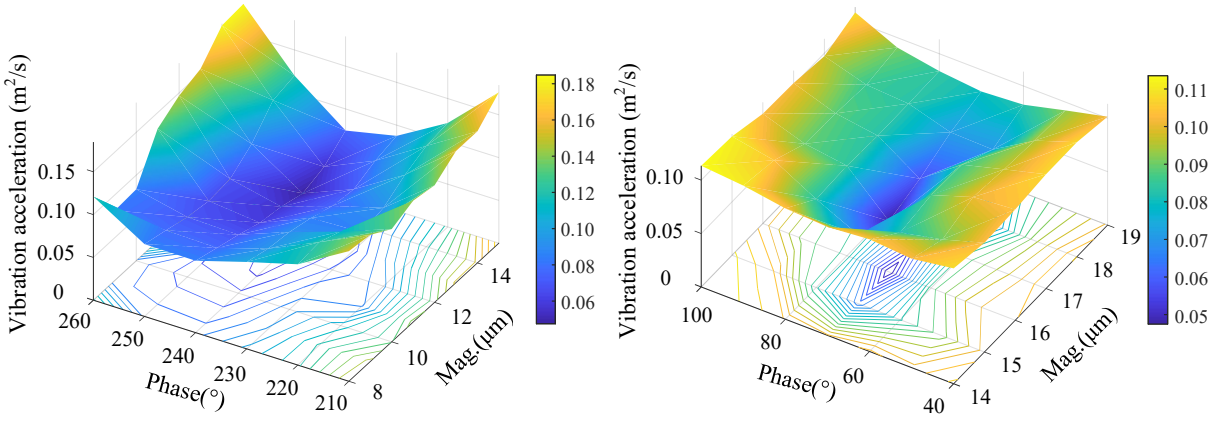


Fig. 7 Rotational frequency vibration acceleration under varying injected sinusoidal amplitude and phase. (a) Only AMB1 was injected. (b) Only AMB2 was injected.

Figure 7 shows the variation in vibration acceleration amplitude at the motor foot's rotational frequency when reference displacement signals, described in (15), are injected into the left and right AMBs. The results indicate that for the injected displacement reference signals, there exists an optimal amplitude and phase that correspond to the minimum vibration acceleration. This indirectly confirms that mechanical processing errors affect control accuracy. When the compensated displacement harmonic amplitude and phase match the error factors, the "zero displacement" control effect is achieved. As discussed in Section II, this results in the minimization of rotor dynamic eccentricity, significantly reducing motor rotational frequency vibrations.

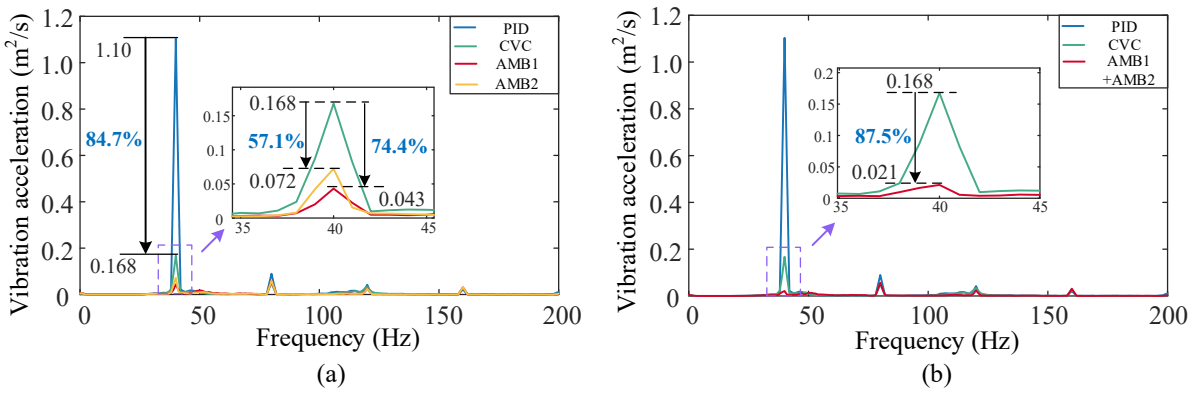


Fig. 8 Vibration acceleration frequency spectrum on motor footings comparing different control strategies. The rotational frequency is 40Hz. (a) Only AMB1 or AMB2 was injected. (b) Simultaneous displacement harmonics injection of two bearings.

Figure 8(a) displays the vibration spectra of the motor foot's acceleration under PID control, CVC, and the proposed displacement vibration control method applied to AMB1 and AMB2. Under PID control, the most prominent vibration line spectrum corresponds to the rotational frequency vibration (40Hz), associated with the dynamic eccentricity of the rotor, as detailed in Section II. Compared to PID control, CVC reduces the vibration amplitude from 1.10 m²/s to 0.168 m²/s, a reduction of 84.7%. However, CVC overlooks the impact of error factors on control precision, leaving room for further optimization.

Through offline testing, we found the optimal compensation values for AMB1 and AMB2, respectively. By injecting displacement harmonics with amplitude and phase values of (13μm, 240°) into radial AMB1 to compensate for error factors, the vibration amplitude is further reduced to 0.043 m²/s, a 74.4% decrease compared to CVC. Similarly, injecting displacement harmonics with amplitude and phase values of (16μm, 70°) into radial AMB2 reduces the vibration amplitude to 0.072 m²/s, a 57.1% reduction compared to CVC.

In previous research, the amplitude of detection errors caused by first-order roundness errors varies from 5 to 20 μm due to different processing techniques (Kim & Lee, 1997; Rossner et al., 2015), and the amplitude of imbalance disturbance is approximately three times that of the first harmonic of sensor runout (Zhang et al., 2021), which closely matches the compensated displacement in our experiment.

When both radial AMBs compensate for displacement harmonics simultaneously, the vibration acceleration spectrum shown in Fig. 8(b) demonstrates a significant improvement. The rotational frequency vibration acceleration is reduced to 0.021 m²/s, representing an 87.5% reduction compared to CVC and a 98.1% reduction compared to PID control.

## 5. Conclusion

This paper presents a vibration suppression strategy based on radial magnetic bearing displacement harmonic injection for AMB-based motor drive systems. The key conclusions are as follows:

*1)* In normal operation of the magnetic bearing, the most significant vibrations are caused by rotor eccentricity at the rotational frequency.

*2)* Measurement errors induced by manufacturing defects and material imperfections, which affect sensor readings, should not be overlooked. These errors degrade the control accuracy of rotor displacement and worsen motor vibrations.

*3)* The proposed vibration control strategy compensates for the error factors in the radial magnetic bearings. Compared to CVC, rotational frequency vibrations are reduced by 87.5%, demonstrating the effectiveness of the proposed approach.

## References


Prasad, K. N. V., and Narayanan, G., Electromagnetic bearings with power electronic control for high-speed rotating machines: Review, analysis, and design example, IEEE Transactions on Industry Applications, Vol.57, No.5 (2021), pp.4946–4957.

Ma, W., Liu, G., Le, Y., and Zheng, S., Stiffness compensation control for centrifugal compressors based on online parameter identification of magnetic bearings, IEEE Transactions on Industrial Electronics, Vol.70, No.9(2023), pp.9421–9431.

Ahad, M. A., and Ahmad, S. M., Investigation of a 2-DOF active magnetic bearing actuator for unmanned underwater vehicle thruster application, Actuators (2021).

Lewis, D. W., Allaire, P. E., and Thomas, P. W., Active magnetic control of oscillatory axial shaft vibrations in ship shaft transmission systems Part 1: System natural frequencies and laboratory scale model, Tribology Transactions, Vol.32, No.2 (1989), pp.170–178.

Peng, C., Zheng, S., Huang, Z., and Zhou, X., Complete synchronous vibration suppression for a variable-speed magnetically suspended flywheel using phase lead compensation, IEEE Transactions on Industrial Electronics, Vol.65, No.7(2018), pp.5837–5846.

Liu, G., Li, J., Zheng, S., Chen, Q., and Liu, H., Suppression of synchronous current using double input improved adaptive notch filter algorithm, IEEE Transactions on Industrial Electronics, Vol.67, No.10(2020), pp.8599–8607.

Ren, G.-P., Zhang, H.-T., Wu, Y., and Ding, H., A general double-input synchronous signal processor for imbalanced vibration mitigation in AMB-rotor systems, IEEE Transactions on Systems, Man, and Cybernetics: Systems (2023), pp.1–10.

Cui, P., Li, S., Zhao, G., and Peng, C., Suppression of harmonic current in active–passive magnetically suspended CMG using improved repetitive controller, IEEE/ASME Transactions on Mechatronics, Vol.21, No.4(2016), pp.2132–2141.

Chuan, M., and Changsheng, Z., Unbalance compensation for active magnetic bearing rotor system using a variable step size real-time iterative seeking algorithm, IEEE Transactions on Industrial Electronics, Vol.65, No.5(2018), pp.4177–4186.

Han, B., Liu, Y., and Zheng, S., Research on vibration suppression for magnetic suspension motor based on repetitive control method, Journal of Vibration, Measurement and Diagnosis, Vol.35, No.3 (2015), pp.486–492.

Chen, S.-L., Lin, S.-Y., and Toh, C.-S., Adaptive unbalance compensation for a three-pole active magnetic bearing system, IEEE Transactions on Industrial Electronics, Vol.67, No.3 (2020), pp.2097–2106.

Sun, H., Jiang, D., and Yang, J., Synchronous vibration suppression of magnetic bearing systems without angular sensors, CES Transactions on Electrical Machines and Systems, Vol.5, No.1 (2021), pp.70–77.

Kim, C.-S., and Lee, C.-W., In situ runout identification in active magnetic bearing system by extended influence coefficient method, IEEE/ASME Transactions on Mechatronics, Vol.2, No.1 (1997), pp.51–57.

Rossner, M., Thuemmel, T., and Ulbrich, H., Online roundness error identification and model-based monitoring for rotors, in Sinha, J. K. (Ed.), Vibration Engineering and Technology of Machinery, Springer, (2015), pp.743–752.

Zhang, H., Liu, J., Zhu, R., Chen, H., and Yuan, H., Nonlinear adaptive harmonics vibration control for active magnetic bearing system with rotor unbalance and sensor runout, IEEE Sensors Journal, Vol.21, No.10 (2021), pp.12245–12254.